Cell Reports

Report

A FOXO-dependent replication checkpoint restricts proliferation of damaged cells

Graphical Abstract

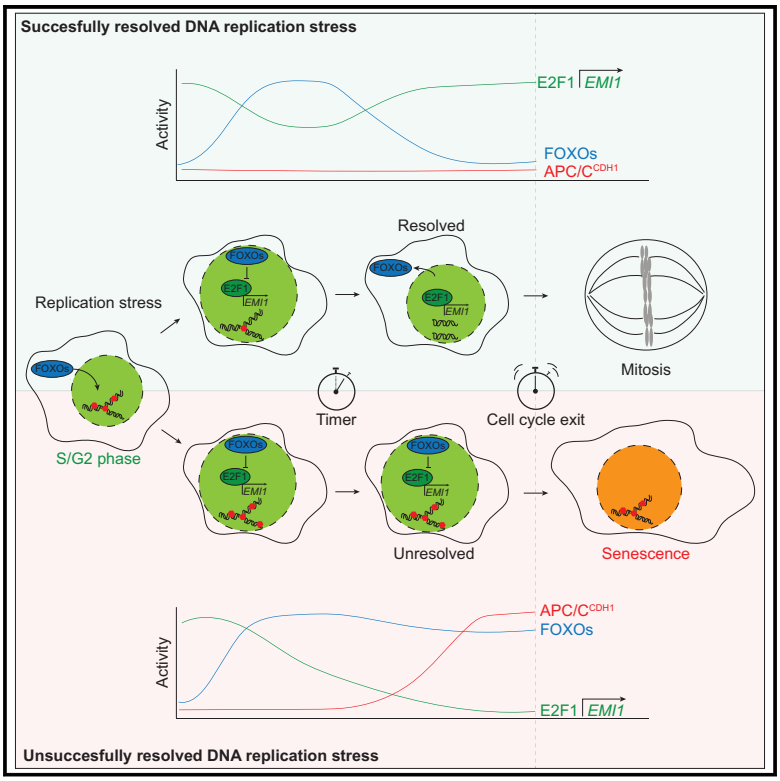

Highlights

- Mild DNA replication stress induces a cell cycle exit from G2 when not resolved
- FOXOs are activated in the DNA replication stress response
- FOXOs function as a timer for DNA replication stress checkpoint reversibility
- FOXO-dependent loss of EMI1 expression causes premature APC/C^{CDH1} activation in G2

Authors

Marten Hornsveld, Femke M. Feringa, Lenno Krenning, ..., Tobias B. Dansen, René H. Medema, Boudewijn M.T. Burgering

Correspondence

m.hornsveld@lumc.nl (M.H.), b.m.t.burgering@umcutrecht.nl (B.M.T.B.)

In Brief

Hornsveld et al. show that reversibility of the DNA replication stress checkpoint is limited via activation of FOXO transcription factors. FOXO activation causes gradual downregulation of APC/C^{CDH1} inhibitor EMI1, which results in cell cycle exit from G2 phase via premature APC/C^{CDH1} activation when mild replication stress is not resolved.

Hornsveld et al., 2021, Cell Reports *34*, 108675
January 26, 2021
https://doi.org/10.1016/j.celrep.2020.108675

CellPress

Cell Reports

CellPress
OPEN ACCESS

Report

A FOXO-dependent replication checkpoint restricts proliferation of damaged cells

Marten Hornsveld,[1,2,6,7,*] Femke M. Feringa,[3,4,6] Lenno Krenning,[3] Jeroen van den Berg,[3,5] Lydia M.M. Smits,[2] Nguyen B.T. Nguyen,[2] Maria J. Rodríguez-Colman,[2] Tobias B. Dansen,[2] René H. Medema,[3] and Boudewijn M.T. Burgering[2,*]
[1]Oncode Institute, Department of Cell and Chemical Biology, Leiden University Medical Center, 2333 Leiden, the Netherlands
[2]Oncode Institute, Center for Molecular Medicine, University Medical Center Utrecht, Utrecht University, 3584 Utrecht, the Netherlands
[3]Oncode Institute, Division of Cell Biology, Netherlands Cancer Institute, 1066 Amsterdam, the Netherlands
[4]Department of Molecular and Cellular Neurobiology, Faculty of Science, Center for Neurogenomics and Cognitive Research, Amsterdam Neuroscience, Vrije Universiteit Amsterdam, 1081 Amsterdam, the Netherlands
[5]Oncode Institute, Hubrecht Institute–KNAW (Royal Netherlands Academy of Arts and Sciences), 3584 Utrecht, the Netherlands
[6]These authors contributed equally
[7]Lead contact
*Correspondence: m.hornsveld@lumc.nl (M.H.), b.m.t.burgering@umcutrecht.nl (B.M.T.B.)
https://doi.org/10.1016/j.celrep.2020.108675

SUMMARY

DNA replication is challenged by numerous exogenous and endogenous factors that can interfere with the progression of replication forks. Substantial accumulation of single-stranded DNA during DNA replication activates the DNA replication stress checkpoint response that slows progression from S/G2 to M phase to protect genomic integrity. Whether and how mild replication stress restricts proliferation remains controversial. Here, we identify a cell cycle exit mechanism that prevents S/G2 phase arrested cells from undergoing mitosis after exposure to mild replication stress through premature activation of the anaphase promoting complex/cyclosome (APC/C^{CDH1}). We find that replication stress causes a gradual decrease of the levels of the APC/C^{CDH1} inhibitor EMI1/FBXO5 through Forkhead box O (FOXO)-mediated inhibition of its transcription factor E2F1. By doing so, FOXOs limit the time during which the replication stress checkpoint is reversible and thereby play an important role in maintaining genomic stability.

INTRODUCTION

Faithful DNA duplication during S phase is crucial for the maintenance of genomic integrity. Stalling or slowing of the replication fork as a result of replication stress leads to formation of aberrant single-stranded DNA (ssDNA) stretches and potentially DNA double-stranded breaks (DSBs). Substantial replication stress may induce gaps, breaks, and micro-deletions at common fragile sites (CFSs) (Glover et al., 1984; Mishmar et al., 1998), highlighting the mutagenic potential of replication stress. Accumulation of ssDNA activates the ATR-dependent DNA replication stress checkpoint response that slows progression from S/G2 to M phase to protect genomic integrity (Zeman and Cimprich, 2014). Nonetheless, mild replication stress can give rise to DNA lesions upon mitotic progression (Harrigan et al., 2011; Lukas et al., 2011). Thus, it is likely that mechanisms are in place to prevent the propagation of under-replicated DNA. Whether and how mild replication stress restricts proliferation remains controversial (Harrigan et al., 2011; Lukas et al., 2011; Koundrioukoff et al., 2013; Arora et al., 2017; Saldivar et al., 2018).

Here, we identify a cell cycle exit mechanism that acts to prevent propagation of damaged DNA following replication stress. We find Forkhead box O transcription factors (FOXOs) are drivers of this cell cycle exit mechanism that limits the time during which the replication stress checkpoint is reversible. FOXO activation following replication stress results in loss of the APC/C^{CDH1} inhibitor EMI1/FBXO5 via repression of its transcriptional regulator E2F1. When EMI1 levels become critically low, the APC/C^{CDH1} is activated, driving S/G2 cells into a G1/G0 state without going through mitosis. Subsequent entrance of senescence ensures protection of genomic integrity.

RESULTS

Replication stress leads to APC^{CDH1} activation in G2 phase

To investigate the cellular response to mild replication stress, we treated non-transformed RPE-1 cells with endogenous-tagged CyclinnB1^{YFP} (RPE-*CCNB1*^{YFP}) and stable expression of *53BP1*^{mCherry} (RPE *CCNB1*^{YFP}-*53BP1*^{mCherry}; Feringa et al., 2016) with aphidicolin (aph) (Figure 1A). Although addition of aph had no effect on cyclin B+ G2 cells, cells that progressed through S phase in the presence of aph showed a clear decrease in mitotic entry (Figure 1B). This decrease in mitotic entry was accompanied by a concomitant increase in cells that abruptly lost cyclin B1 expression (Figures 1A and 1C). Based on previous findings (Krenning et al., 2014), we hypothesized that loss of cyclin B1 expression may correspond to levels of DNA damage.

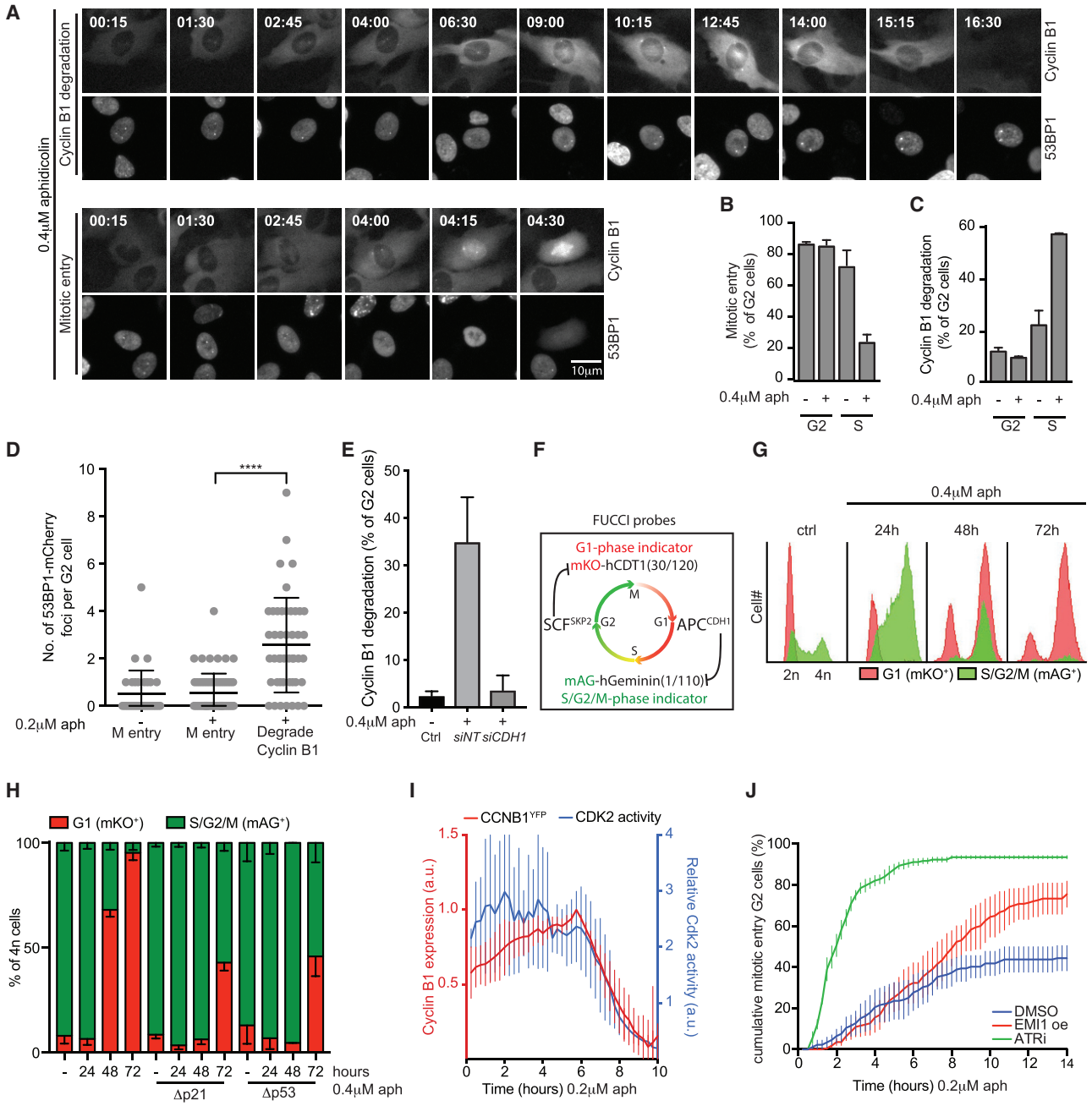

Figure 1. Replication stress leads to APC^{CDH1} activation in G2 phase

(A) Time-lapse movie stills of RPE CCNB^{YFP}–53BP1^{mCherry} cells treated with aphidicolin (aph).

(B) Mitotic entry of G2 cells (cyclin B1 positive at t = 0) or S phase cells (cyclin B1 positive at t = 15) in response to aph. n = 3; mean ± SEM.

(C) Percentage of cells that degrade cyclin B1 in response to aph. n = 3; mean ± SEM.

(D) 53BP1 foci in G2 cells before cyclin B1 degradation or mitotic entry. Dots represent individual cells n > 31 pooled from 2 independent experiments. Mean ± SD. ****p < 0.0001 (Welch's corrected unpaired t test).

(E) Percentage of aph-treated G2 cells that degrade cyclin B1 in presence of *siCDH1*; n = 3; mean ± SD.

(F) hCDT1-mKO2, degraded by SCF^{SKP2} in S/G2/M phases, indicates G1 phase. hGeminin-mAG, degraded by APC/C^{CDH1} in G1 phase, indicates S/G2/M phases.

(G) Cell cycle and DNA content distribution after aph. Red: G1; green: S/G2/M.

(H) Quantification of cell cycle distribution of 4n cells knockout for p53 (Δp53) and (Δp21); n = 3; mean ± SD.

(I) Relative CDK2 activity and cyclin B1^{YFP} intensity in individual G2 cells. Lines represent mean of n = 16 cells from two independent experiments ± 95% confidence interval (CI).

(J) Cumulative mitotic entry of EMI1-overexpressing or ATR-inhibitor-treated G2 cells after aph. n = 3; mean ± SEM.

Indeed, cells that degrade cyclin B1 in response to mild replication stress display increased 53BP1 foci compared to control cells or cells that recovered from replication stress and progressed to mitosis (Figure 1D). Importantly, abrogation of DNA damage signaling by ATR inhibition caused an increase in 53BP1 foci number in G1 daughter cells (Figure S1A), indicative of mitotic progression in the presence of under-replicated DNA (Harrigan et al., 2011; Lukas et al., 2011).

We and others have previously shown that loss of cyclin B1 and other cell cycle targets after DNA double-stranded breaks (DSBs) is mediated via APC/C^{CDH1}-dependent protein degradation, causing cells to enter a state of senescence (Sudo et al., 2001; Wiebusch and Hagemeier, 2010; Krenning et al., 2014). To examine whether aph-induced loss of cyclin B1 is caused by APC/C^{CDH1} activation, we depleted CDH1. Indeed, CDH1 knockdown prevented replication-stress-induced cyclin B1 degradation (Figures 1E and S1B). Experiments using RPE-1 cells stably expressing fluorescent ubiquitination-based cell cycle indicator (FUCCI) probes (Sakaue-Sawano et al., 2008; Figure 1F) confirmed that the observed APC/C^{CDH1} activation upon aph treatment occurred in G2. Aph treatment of RPE-FUCCI and U2OS-FUCCI cells resulted in accumulation of 4n G1 (mKO2+) cells over time, showing that these cells activate APC/C^{CDH1} without going through mitosis (Figures 1G and S1C). We and others previously demonstrated that an APC/C^{CDH1}-dependent cell cycle exit in response to DSBs in G2 phase is caused by p53-dependent p21 expression (Wiebusch and Hagemeier, 2010; Krenning et al., 2014). Interestingly, we observe that APC/C^{CDH1} activation in response to mild replication stress is delayed, but not abrogated, in p21 (Δp21) and p53 (Δp53) knockout RPE-FUCCI cells (Figure 1H).

In G2, activation of APC^{CDH1} is prevented by CDK1/2-dependent phosphorylation of CDH1 (Zachariae et al., 1998; Kramer et al., 2000). To characterize CDK activity following replication stress, we used the previously described CDK2 activity sensor in RPE *CCNB*^{YFP} cells (Spencer et al., 2013). We found, in aph-treated G2 cells, CDK2 activity was stable until it dropped in synchrony with cyclin B1 (Figure 1I). The simultaneous loss of CDK2 activity and APC/C^{CDH1} target cyclin B1 is surprising, because APC/C^{CDH1} activation in response to DSBs is preceded by loss of CDK activity (Sudo et al., 2001; Lee et al., 2009; Wiebusch and Hagemeier, 2010; Krenning et al., 2014; Müllers et al., 2014; Feringa et al., 2016). Therefore, we expected CDK2 activity to drop before cyclin B1, yet our results implicate that APC/C^{CDH1} can be activated despite the presence of CDK2 activity.

In addition to CDK1/2-mediated inhibition, EMI1 blocks APC/C^{CDH1} activity during S/G2 and loss of EMI1 is sufficient for premature activation of APC/C^{CDH1} in G2 (Reimann et al., 2001; Hsu et al., 2002; Miller et al., 2006; Di Fiore and Pines, 2007; Lee et al., 2009). We therefore equipped our RPE *CCNB*^{YFP}-*53BP1*^{mCherry} cells with doxycycline-inducible EMI1 overexpression (Feringa et al., 2016) to define the importance of EMI1 loss for APC/C^{CDH1} activation following replication stress. Overexpression of EMI1 prevented cyclin B1 degradation and rescued mitotic entry of cells exposed to replication stress (Figures 1J and S1D). As replication stress results predominantly in ATR/CHK1-activating lesions (Saldivar et al., 2017), this raises the question whether sustained ATR signaling is required to maintain cells arrested and induce cell cycle exit. To address this, we treated G2 cells that progressed through S phase in the presence of aphidicolin with ATR inhibitor. ATR inhibition prevented cyclin B1 degradation and resulted in immediate mitotic entry of almost all G2 cells that progressed through S phase in presence of aph (Figures 1J and S1D). In contrast, aph-treated cells that did recover from replication stress in the DMSO-treated condition showed a clear delay in mitotic entry (Figure 1J). Rescue by ATR inhibition was distinct from rescue with EMI1 overexpression, because EMI1 expressing G2 cells still arrested for several hours before mitotic progression. These results show sustained ATR activity maintains the G2 arrest and loss of EMI1 is ultimately required for APC/C^{CDH1}-dependent cell cycle exit. Together, these results imply there are additional players to p53/p21 or cyclin B/CDK1/2 signaling in the replication stress checkpoint that steer the decision between proliferation or cell cycle exit.

FOXO3 is activated by replication stress and induces cell cycle exit from G2 phase

DNA damage results in the activation of a transcriptional program that promotes DNA repair and stalls cell cycle progression (Rashi-Elkeles et al., 2014). To determine which transcriptional programs are induced by replication stress, we determined the transcriptome of aph-treated cells. Upon replication stress, we identified 272 differentially expressed genes (Figure 2A). Transcription factor binding site (TFBS) analysis revealed a significant enrichment of FOXO TFBSs in promoters of differentially expressed genes (Figures S2A–S2C). As FOXOs are known regulators of cell cycle arrest and are involved in the DNA damage response (Brown and Webb, 2018) (Hornsveld et al., 2018b), we determined whether FOXOs are activated by replication stress. Indeed, we observed an increase in nuclear FOXO3, specifically in S/G2 phase cells already at 2 h after aph treatment (Figures 2B and 2C). Although FOXOs usually function redundantly and mRNA expression of *FOXO1*, *FOXO3*, and *FOXO4* increases after aph treatment, FOXO4 protein is undetectable in RPE cells (Charitou et al., 2015) and FOXO1 localization was hardly affected by aph treatment, suggesting a more dominant role for FOXO3 (Figures S3A and S3B). Nuclear translocation of FOXO3 was reduced after ATR inhibition, showing ATR affects FOXO3 activation during replication stress (Figures 2C and S3C).

To study whether nuclear localization of FOXO is sufficient to cause premature APC/C^{CDH1} activation, we introduced a doxycycline-inducible, constitutively nuclear mutant of FOXO3 (FOXO3.A3) in RPE-FUCCI cells (Figure S3D) and analyzed cell fate after FOXO3.A3 expression. FOXOs are known to induce a robust G1 cell cycle arrest, and therefore, only cells in early S/G2 at the time of FOXO3.A3 induction were included in our analysis (Medema et al., 2000). Cells arrest for 15–35 h in S/G2 phase upon FOXO3.A3 expression before prematurely activating the APC/C^{CDH1}, much like the response to replication stress (Figure 2D). We found that 74% ± 4% of all 4n RPE-FUCCI cells lost the S/G2 indicator and were G1 indicator positive at 30 h after doxycycline-induced FOXO3.A3 expression (Figures 2E and S3E), indicative of APC/C^{CDH1} activation and cell cycle exit from G2 without mitosis. This response to FOXO3.A3 expression is conserved in SKBR3 and MCF7 cells (Figures S4A and S4B). Interestingly, we observed that FOXO3.A3 expression did not

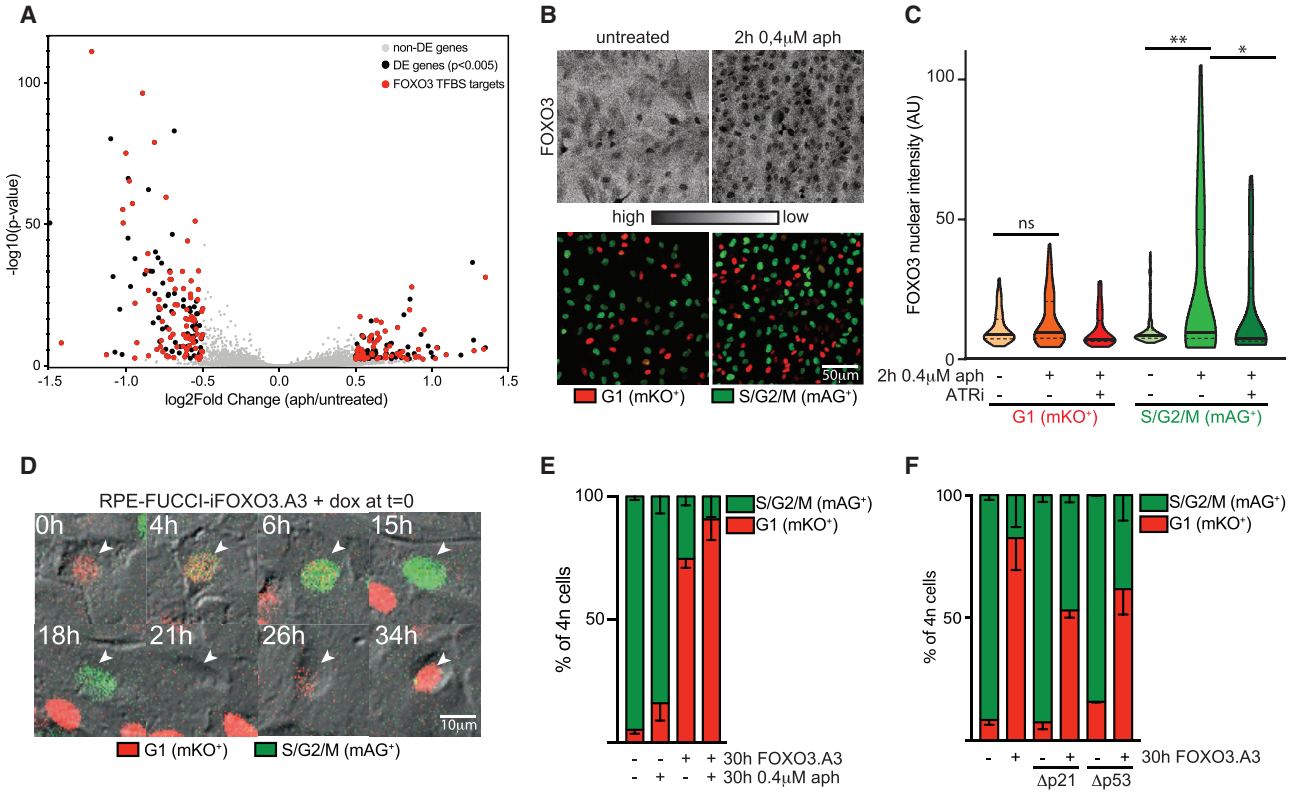

Figure 2. FOXO3 is activated by replication stress and induces cell cycle exit from G2 phase

(A) mRNA sequencing volcano plot of differentially expressed (DE) genes after 7 h aph. non-DE, gray; DE, black; DE genes with ≥1 FOXO transcription factor binding site, red).

(B) FOXO3 (black) expression and localization. Red: mKO+; green: mAG+.

(C) FOXO3 mean nuclear intensity after aph and ATR inhibitor. n ≥ 179 cells pooled from 2 independent experiments; median ± quartile. *p < 0.05; **p < 0.005 (Welch's corrected unpaired t test).

(D) Time-lapse stills of cell cycle exit 18 h after FOXO3.A3.

(E and F) Cell cycle and DNA content distribution of Δp53 and Δp21 cells after 30 h FOXO3.A3 expression and/or aph. Red: G1; green: S/G2/M; n = 3; mean ± SD.

induce p53 or p21 expression and also caused APC/C^{CDH1} activation in S/G2 phase in Δp53 and Δp21 cells (Figures 2F and S4C–S4E). Collectively, these observations imply that FOXOs promote premature APC/C^{CDH1} activation in response to replication stress.

FOXOs support replication stress response and cooperate with p53/p21 to induce cell cycle exit

To test whether FOXOs are required for replication-stress-induced APC/C^{CDH1} activation and whether this is dependent on p21 or p53, we equipped RPE-FUCCI, Δp21, and Δp53 cells with a doxycycline-inducible short hairpin RNA (shRNA) known to efficiently reduce *FOXO1* and *FOXO3* expression (de Keizer et al., 2010; Shats et al., 2013) (Hornsveld et al., 2018a). Replication stress induced the expression of p21 in a p53-dependent manner, and both p53 and p21 expressions are reduced in the absence of FOXOs, in unperturbed conditions as well as after aph treatment (Figure 3A). Although aph-induced cell cycle exit is not solely dependent on p21/p53 activation (Figures 1H and 3B), FOXO depletion did fully impair aph-induced APC/C^{CDH1} activation in G2 (Figures 3B and S4F). Loss of FOXOs lowered the activity of CHK1 and CHK2 in response to aph and other DNA-damaging agents, like hydroxyurea (HU) and neocarzinostatin (NCS) (Figure 3C), but did not prevent initial DNA damage signaling, as FOXO depletion did not significantly reduce pATM levels or γH2AX foci in response to aph treatment (Figures 3C and 3D). Downstream events, such as the loading of monoubiquitinated FANCD2 and the establishment of 53BP1 foci in S/G2 cells following replication stress, were perturbed in the absence of FOXOs (Figures 3E–3G). Together, these results delineate an important role for FOXOs in both replication checkpoint activation and subsequent cell cycle exit. The central role of FOXOs in the replication stress response suggests that reduced FOXO expression might increase resistance to aph treatment. Indeed, loss of FOXOs increased the IC_{50} of aph in RPE-FUCCI cells by ~54% (Figure 3H). Taken together, we uncover FOXOs as important players in replication stress.

FOXOs activate APC^{CDH1} in G2 by downregulating EMI1

Next, we addressed what events downstream of FOXOs may contribute to the cellular response to mild replication stress. Our data show FOXOs regulate APC/C^{CDH1} activation following

CellPress
OPEN ACCESS

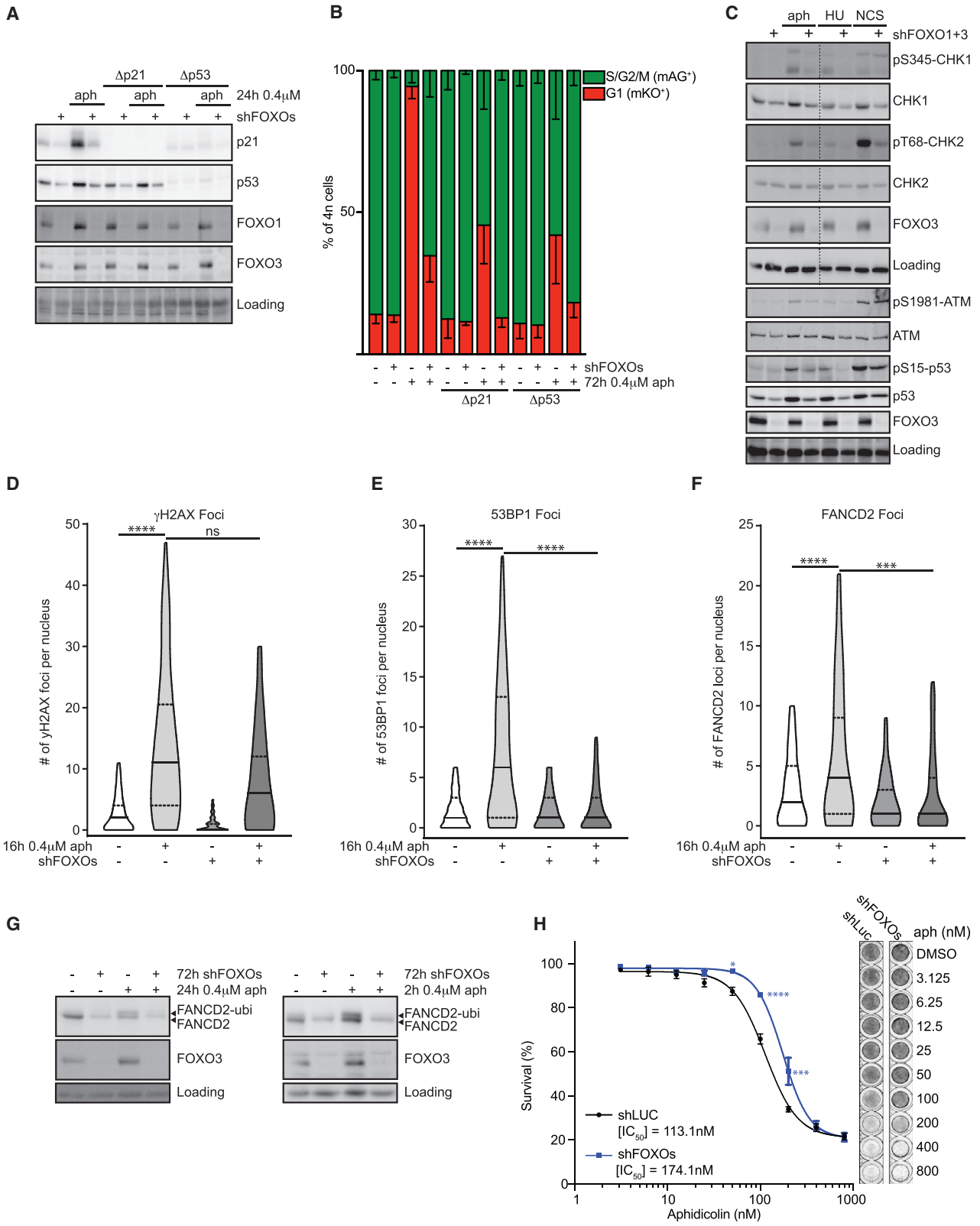

(legend on next page)

replication stress. Indeed, we observed that FOXO3.A3-induced S/G2 cell cycle exit is impaired upon CDH1 knockdown (Figures S5A–S5C). In addition, FOXO3.A3 expression results in a gradual decrease in EMI1 expression in asynchronously cultured RPE, SKBR3, and MCF7 cells, which is in line with previous studies showing that EMI1 downregulation is a prerequisite for cell cycle exit in G2 phase (Figures 4A, S5D, and S5E; Lee et al., 2009; Wiebusch and Hagemeier, 2010). To exclude that EMI1 downregulation is not merely the effect of a FOXO-induced G1 arrest or APC/C^{CDH1}-mediated degradation (Cappell et al., 2018), we sorted cells based on G1 and S/G2/M indicator expression 8 and 16 h after FOXO3.A3 induction. As expected, EMI1 expression was not detected in G0/G1 phase and highly expressed in S/G2 phases in control cells (Figures 4B and 4C). FOXO3.A3 induction diminished EMI1 mRNA and protein expression in S/G2 phase cells (Figures 4B and 4C). Accordingly, cells were sensitized to exit the cell cycle when EMI1 knockdown was combined with FOXO3.A3 expression (Figures 4D and S5F). To determine whether forced EMI1 expression can prevent FOXO3-induced premature APC/C^{CDH1} activation, we constructed RPE-FUCCI cells with doxycycline-inducible FOXO3.A3 and mTurq2-EMI1 (Figure 4E; Feringa et al., 2016). Although FOXO3.A3 expression reduced mitotic entry of G2 cells due to premature APC/C^{CDH1} activation (Figure 4F), simultaneous expression of EMI1 prevented APC/C^{CDH1} activation in G2 and subsequently arrested at metaphase as a consequence of high EMI1 levels in mitosis (Figures 4F and S5G; Margottin-Goguet et al., 2003).

We noticed endogenous EMI1 levels still decreased in FOXO3.A3- and EMI1-overexpressing cells (Figure 4E), suggesting transcriptional repression by FOXOs is responsible for reduced endogenous EMI1 expression. If FOXOs regulate EMI1 levels in S/G2 phase in response to replication stress, loss of FOXOs should stabilize EMI1 levels. Indeed, aph-induced loss of EMI1 in S/G2 phase cells is prevented upon FOXO depletion (Figures 4G and 4H). Hence, we conclude that FOXO-induced APC/C^{CDH1} activation is mediated via repression of *EMI1*.

Although ~20% of all genes in the genome harbor FOXO-binding elements in their promoter, FOXO TFBSs are absent in the *EMI1* promoter, implying *EMI1* transcription is likely not regulated by FOXO binding directly to the *EMI1* promoter (Eijkelenboom et al., 2013a, 2013b; Brown and Webb, 2018). This is in line with observations that FOXOs are dominantly transcriptional activators (Eijkelenboom et al., 2013a, 2013b; Webb et al., 2013; Brown and Webb, 2018). The main transcription factor driving *EMI1* expression is E2F1 (Hsu et al., 2002), and although the *E2F1* promoter region also does not contain FOXO TFBSs, previous studies have shown FOXOs can bind to E2F1 and thereby alter E2F1 target gene expression (Shats et al., 2013). Indeed, co-immunoprecipitation (coIP) using GFP-FOXO1/3 and HA-E2F1 confirmed that FOXOs can bind to E2F1 (Figure S6A). To test whether FOXOs indeed affect E2F1-dependent transcription of *EMI1* and other E2F1 target genes, we performed chromatin immunoprecipitation (ChIP). We found binding of endogenous E2F1 to the promoters of *EMI1* as well as cyclin E (*CCNE2*) and A (*CCNA2*) was reduced when FOXO3.A3 was expressed (Figure 4I). Accordingly, expression of E2F1 target genes, *E2F1* itself, *CCNE2*, and *CCNA2* was reduced (Figures S6B–S6D). Indeed, FOXO-induced APC/C^{CDH1} activation is enhanced when cells enter S phase with lowered E2F1 levels, as partial *E2F1* knockdown synergizes with FOXO3.A3 expression to activate APC/C^{CDH1} in S/G2 (Figures 4J, 4K, and S6E).

Next, we determined whether cells that activate APC/C^{CDH1} in G2 truly switch to a G0/G1 state after EMI1 downregulation. To this end, we sorted RPE-FUCCI-FOXO3.A3 cells based on G1 and S/G2/M indicator expression and DNA content at 24 h after FOXO3.A3 induction (Figure 4L). 2n G1 cells reflect G1 as EMI1 levels and RB phosphorylation are low, cyclin D is high, and both cyclin A and B are absent. FOXO3.A3 expression in 2n G1 cells induced expression of its target p27 and reduced the expression of cyclin D, known to lead to a G1 arrest (Medema et al., 2000). In 4n S/G2/M cells, the expression of EMI1, cyclin A, cyclin B, SKP2, CDH1, and phosphorylation of RB are high, confirming that these cells are indeed in S/G2 phase. Strikingly, FOXO3.A3 expression reduced EMI1 expression in S/G2 cells, illustrating that FOXO-mediated EMI1 repression precedes APC/C^{CDH1} activation. Additionally, p27 and p21 are not induced, in line with the fact that SCF^{SKP2} mediates their degradation in S/G2 cells (Nakayama et al., 2000, 2004). Importantly, 4n G1 cells resemble 2n G1 cells, as expression of EMI1, cyclin A, cyclin B, SKP2, and phosphorylation of RB are absent. The high p27 and p21 levels in 4n G1 cells suggest that these cells are arrested. This experiment also confirms our initial observation that APC/C^{CDH1} activation is not preceded by CDK inhibition, as p27 and p21 induction succeeds APC/C^{CDH1} activation. To assess the nature of the arrest, we analyzed cells 10 days after mild replication stress and FOXO3.A3 expression. Treatment of RPE cells with aph decreases cell proliferation and resulted in appearance of β-galactosidase and p21-positive, lamin-B-negative senescent cells. This replication-stress-induced senescence was reduced after shFOXO expression (Figures S7A and S7B). Collectively, these data show that FOXO-dependent premature activation of the APC/C^{CDH1} prevents mitotic entry and instead pushes cells into a 4n senescent state.

Figure 3. FOXOs support replication stress response and cooperate with p53/p21 to induce cell cycle exit

(A) p21, p53, FOXO1, and FOXO3 protein levels in Δp21 and Δp53 cells after aph and shFOXOs.

(B) Cell cycle distribution of Δp21 and Δp53 cells after aph and shFOXOs. Red: G1; green: S/G2/M. n = 3; mean ± SD.

(C) Phospho-CHK1, CHK1, phospho-CHK2, CHK2, phospho-ATM, ATM, phospo-p53, p53, and FOXO3 levels after aph, hydroxyurea (HU), or neocarcinostatin (NCS).

(D–F) Immunofluorescence quantification of γH2AX, 53BP1, and FANCD2 foci in control (n = 821; n = 1,553; n = 821), aph (n = 88; n = 1,059; n = 273), shFOXOs (n = 191; n = 801; n = 116), and combined aph + shFOXOs (n = 71; n = 1,639; n = 655)-treated cells. Median ± quartiles ***$p < 0.0005$; ****$p < 0.00005$ (Welch's corrected unpaired t test).

(G) Mono-ubiquitinated FANCD2 and FOXO3 levels after aph and shFOXOs. Nonspecific background staining was used as loading control.

(H) Cell viability after aph, shLuc, and shFOXOs for 7 days. n = 3; mean ± SEM. Bonferroni multiple testing corrected ANOVA *$p < 0.05$; ***$p < 0.005$; ****$p < 0.0005$.

CellPress
OPEN ACCESS

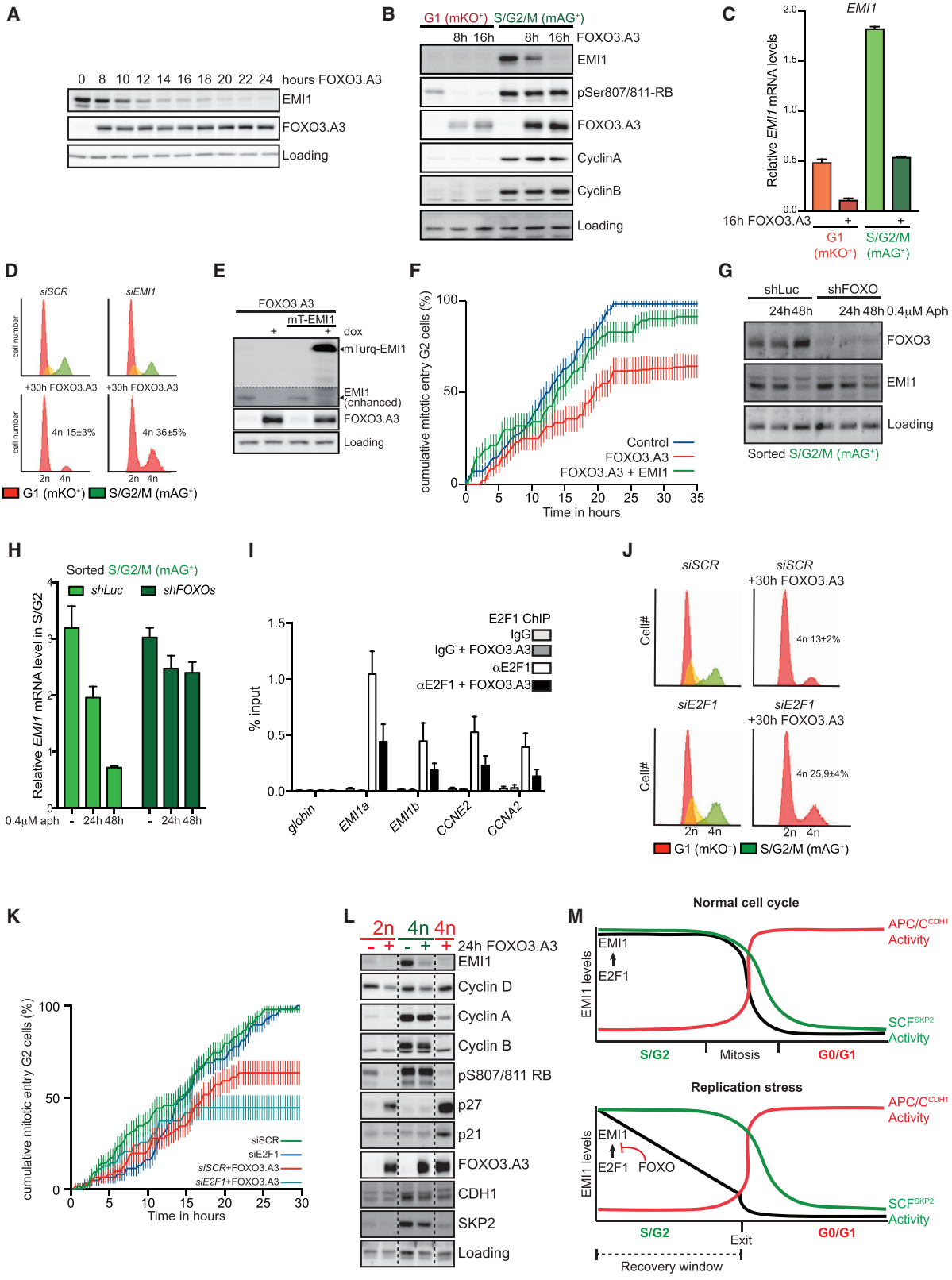

(legend on next page)

DISCUSSION

Our observations expand on earlier work showing that both transformed and non-transformed cells that experience very low levels of replication stress progress through mitosis, resulting in replication in mitosis or chromosomal aberrations and 53BP1 foci in G1 phase (Harrigan et al., 2011; Lukas et al., 2011; Koundrioukoff et al., 2013; Minocherhomji et al., 2015). Here, we extended these findings and show that slightly higher levels (but still very low) of replication stress cause the formation of 53BP1 bodies in G2 phase and prevent mitotic entry through a FOXO-dependent checkpoint mechanism. Together, these results argue for a threshold-based response following replication stress. In addition, increased 53BP1 bodies in non-transformed "G1" cells following replication stress were previously shown based on cyclin A negativity (Harrigan et al., 2011; Lukas et al., 2011). Although these results were interpreted as all being post-mitotic G1 cells, our data show that these cells could also be 4n G1/G0 cells, resulting from premature APC/C^{Cdh1} activation. We find that FOXO3-dependent cell cycle exit also occurs in transformed cells, albeit at a lower efficiency. The reduced efficiency of cell cycle exit in transformed cells could be caused by impairment of p53 signaling (Kleiblova et al., 2013).

In agreement with previous reports, we show that G2 phase can be extended in an ATR-dependent manner, to provide time for DNA repair (Koundrioukoff et al., 2013). However, if repair is not successful within ~24 h, APC/C^{CDH1} is activated and cells exit the cell cycle. It has previously been shown that DSBs in G2 phase may cause premature APC/C^{CDH1} activation, resulting in irreversible withdrawal from the cell cycle (Sudo et al., 2001; Lee et al., 2009; Wiebusch and Hagemeier, 2010; Krenning et al., 2014; Feringa et al., 2016). Premature APC/C^{CDH1} activation is preceded by p21-dependent nuclear entrapment of cyclin B1-CDK complexes, which renders it inert for CDK (re-)activation (Krenning et al., 2014; Müllers et al., 2014). Intriguingly, here, we find that CDK2 remains active during a replication-stress-induced G2 arrest and that APC/C^{CDH1} can be activated independent from p53, p21, or CDK2 inhibition. This means that APC/C^{CDH1} can be activated in cells containing active CDK complexes. We find that ATR-dependent FOXO activation acts as a timer to restrict the window in which cells may recover from replication stress, by gradually decreasing EMI1 levels through removing E2F1 from the *EMI1* promoter (Figure 4M). Alteration of E2F1-dependent transcriptional output by FOXOs has been reported previously for pro-apoptotic genes, and we now show this mechanism is also applicable to cell cycle regulation in S/G2 phase (Shats et al., 2013).

Interestingly, FOXOs and p53/p21 cooperate to restrict replication stress recovery time. On one hand, FOXOs support the checkpoint and sensitize the APC/C^{CDH1} to activation; on the other hand, p21 inhibits CDK activity. Combined, this results in a robust switch that can revert the cell from a S/G2 state into senescence. Next to indirectly regulating the APC/C^{CDH1}, we observed that FOXOs are required for replication stress checkpoint establishment; hence, FOXO depletion results in reduced downstream p53/p21 induction. Induction of p53/p21 is absent upon FOXO3.A3 expression, indicating FOXOs and p53/p21 can act independently after replication stress. The effect of FOXO depletion on downstream DNA damage signaling suggests a role for FOXO in DNA damage response and checkpoint activation. We show that nuclear accumulation of FOXO following replication stress depends on ATR, yet a direct interaction between ATR and FOXO activation remains to be determined. This is of great interest for future studies and could be related to the previously suggested role for FOXOs in ATM/CHK2-mediated DSB repair (Tsai et al., 2008; Chung et al., 2012; Adamowicz et al., 2016).

Noteworthy, FOXOs have been suggested to play a role in inducing a G2 arrest, but these conclusions were based solely on DNA content analysis (Alvarez et al., 2001; Furukawa-Hibi et al., 2002; Schmidt et al., 2002; Tran et al., 2002). As we do not observe mAG+ cells after FOXO activation, it is tempting to speculate that the previously reported FOXO-induced G2 arrest in fact represent cells that exited G2 and are in a G0/G1 or senescent state with a 4n DNA content.

Combined, our results establish a role for FOXOs in the replication stress response. FOXOs cooperate with ATR/CHK1 and p53/p21 both by supporting checkpoint establishment and restricting time to resolve damaged DNA. Importantly, deregulation of this FOXO-driven timer gives cells the opportunity to divide with higher levels of replication stress, potentially promoting cellular transformation.

Figure 4. FOXOs activate APC^{CDH1} in G2 by downregulating EMI1

(A) EMI1 and FOXO3.A3 expression in asynchronous cells harvested at the same time. Nonspecific background staining was used as loading.
(B) EMI1, phospho-RB, FOXO3, cyclin A, and cyclin B in mKO+ and mAG+ sorted cells after FOXO3.A3 expression.
(C) *EMI1* expression in mKO+ and mAG+ sorted cells after FOXO3.A3 expression. n = 3; mean ± SD.
(D) Cell cycle distribution after FOXO3.A3 expression and *siEMI1*. n = 3. Red: G1; green: S/G2/M.
(E) EMI1, mTurq2-EMI1, and FOXO3.A3 protein levels.
(F) Cumulative mitotic entry of G2 cells after FOXO3.A3 and EMI1 overexpression. n = 3; mean ± SEM.
(G) EMI1 and FOXO3.A3 levels in mAG+ sorted cells after aph.
(H) *EMI1* expression in mAG+ sorted cells after FOXO3.A3 expression. n = 3; mean ± SD.
(I) Chromatin immunoprecipitation (ChIP) qPCR of genomic E2F1 binding sites in 2 promoter regions of *EMI1* (EMI1a and Emi1b), *CCNE2*, and *CCNA2* after FOXO3.A3 expression; n = 3; mean ± SD.
(J) Cell cycle distribution after FOXO3.A3 and *siE2F1* expression. n = 3; mean ± SD.
(K) Cumulative mitotic entry of G2 cells after FOXO3.A3, *siSCR*, and *siE2F1* expression. n = 3; mean ± SEM.
(L) EMI1, cyclin B, cyclin A, cyclin D, phospho-RB, p27, p21, FOXO3, CDH1, and SKP2 levels in 2n G1, 4n S/G2/M, and 4n G1 sorted cells after FOXO3.A3 expression.
(M) Schematic illustrating FOXOs reduce EMI1 levels in response to replication stress. When EMI1 levels reach critically low levels, the APC/C^{CDH1} (red line) is activated, SCF^{SKP2} (green line) inactivated, and cell cycle exit from G2 is triggered.

CellPress
OPEN ACCESS

STAR★METHODS

Detailed methods are provided in the online version of this paper and include the following:

- KEY RESOURCES TABLE
- RESOURCE AVAILABILITY
  - Lead contact
  - Materials availability
  - Data and code availability
- EXPERIMENTAL MODEL AND SUBJECT DETAILS
  - Cell lines and generation of cell lines
  - Constructs, lentiviral transduction and transfections
- METHOD DETAILS
  - Immunoblotting and antibodies
  - Immunofluorescence
  - RT-qPCR
  - Flow cytometry
  - Live cell imaging and tracking
  - mRNA sequencing and Analysis
- QUANTIFICATION AND STATISTICAL ANALYSIS

SUPPLEMENTAL INFORMATION

Supplemental Information can be found online at https://doi.org/10.1016/j.celrep.2020.108675.

ACKNOWLEDGMENTS

This study is financially supported by CancerGenomicsCenter.nl, the Oncode Institute, and the research grants UU2014-6902, UU2009-4490 (to T.B.D.), and NKI2017-6787 (to R.H.M.) from the Dutch Cancer Society (KWF kankerbestrijding).

AUTHOR CONTRIBUTIONS

M.H., F.M.F., L.K., L.M.M.S., J.v.d.B., and B.M.T.B. performed experiments. M.H., F.M.F., L.K., and J.v.d.B. wrote the manuscript. N.B.T.N. and M.J.R.-C. supported cell sorting. T.B.D., R.H.M., and B.M.T.B. financially supported this study and provided critical feedback.

DECLARATION OF INTERESTS

The authors declare no competing interests.

Received: January 31, 2020
Revised: October 30, 2020
Accepted: December 30, 2020
Published: January 26, 2021

REFERENCES

Adamowicz, M., Vermezovic, J., and d'Adda di Fagagna, F. (2016). NOTCH1 inhibits activation of ATM by impairing the formation of an ATM-FOXO3a-KAT5/Tip60 complex. Cell Rep. *16*, 2068–2076.

Alvarez, B., Martínez-A, C., Burgering, B.M., and Carrera, A.C. (2001). Forkhead transcription factors contribute to execution of the mitotic programme in mammals. Nature *413*, 744–747.

Arora, M., Moser, J., Phadke, H., Basha, A.A., and Spencer, S.L. (2017). Endogenous replication stress in mother cells leads to quiescence of daughter cells. Cell Rep. *19*, 1351–1364.

Blomen, V.A., Májek, P., Jae, L.T., Bigenzahn, J.W., Nieuwenhuis, J., Staring, J., Sacco, R., van Diemen, F.R., Olk, N., Stukalov, A., et al. (2015). Gene essentiality and synthetic lethality in haploid human cells. Science *350*, 1092–1096.

Brown, A.K., and Webb, A.E. (2018). Regulation of FOXO factors in mammalian cells. Curr. Top. Dev. Biol. *127*, 165–192.

Cappell, S.D., Mark, K.G., Garbett, D., Pack, L.R., Rape, M., and Meyer, T. (2018). EMI1 switches from being a substrate to an inhibitor of APC/C^{CDH1} to start the cell cycle. Nature *558*, 313–317.

Charitou, P., Rodriguez-Colman, M., Gerrits, J., van Triest, M., Groot Koerkamp, M., Hornsveld, M., Holstege, F., Verhoeven-Duif, N.M., and Burgering, B.M. (2015). FOXOs support the metabolic requirements of normal and tumor cells by promoting IDH1 expression. EMBO Rep. *16*, 456–466.

Chung, Y.M., Park, S.H., Tsai, W.B., Wang, S.Y., Ikeda, M.A., Berek, J.S., Chen, D.J., and Hu, M.C. (2012). FOXO3 signalling links ATM to the p53 apoptotic pathway following DNA damage. Nat. Commun. *3*, 1000.

Cong, L., Ran, F.A., Cox, D., Lin, S., Barretto, R., Habib, N., Hsu, P.D., Wu, X., Jiang, W., Marraffini, L.A., and Zhang, F. (2013). Multiplex genome engineering using CRISPR/Cas systems. Science *339*, 819–823.

de Keizer, P.L.J., Packer, L.M., Szypowska, A.A., Riedl-Polderman, P.E., van den Broek, N.J., de Bruin, A., Dansen, T.B., Marais, R., Brenkman, A.B., and Burgering, B.M. (2010). Activation of forkhead box O transcription factors by oncogenic BRAF promotes p21cip1-dependent senescence. Cancer Res. *70*, 8526–8536.

Di Fiore, B., and Pines, J. (2007). Emi1 is needed to couple DNA replication with mitosis but does not regulate activation of the mitotic APC/C. J. Cell Biol. *177*, 425–437.

Eijkelenboom, A., Mokry, M., Smits, L.M., Nieuwenhuis, E.E., and Burgering, B.M. (2013a). FOXO3 selectively amplifies enhancer activity to establish target gene regulation. Cell Rep. *5*, 1664–1678.

Eijkelenboom, A., Mokry, M., de Wit, E., Smits, L.M., Polderman, P.E., van Triest, M.H., van Boxtel, R., Schulze, A., de Laat, W., Cuppen, E., and Burgering, B.M. (2013b). Genome-wide analysis of FOXO3 mediated transcription regulation through RNA polymerase II profiling. Mol. Syst. Biol. *9*, 638.

Feringa, F.M., Krenning, L., Koch, A., van den Berg, J., van den Broek, B., Jalink, K., and Medema, R.H. (2016). Hypersensitivity to DNA damage in antephase as a safeguard for genome stability. Nat. Commun. *7*, 12618.

Furukawa-Hibi, Y., Yoshida-Araki, K., Ohta, T., Ikeda, K., and Motoyama, N. (2002). FOXO forkhead transcription factors induce $G_{(2)}$-M checkpoint in response to oxidative stress. J. Biol. Chem. *277*, 26729–26732.

Glover, T.W., Berger, C., Coyle, J., and Echo, B. (1984). DNA polymerase α inhibition by aphidicolin induces gaps and breaks at common fragile sites in human chromosomes. Hum. Genet. *67*, 136–142.

Harrigan, J.A., Belotserkovskaya, R., Coates, J., Dimitrova, D.S., Polo, S.E., Bradshaw, C.R., Fraser, P., and Jackson, S.P. (2011). Replication stress induces 53BP1-containing OPT domains in G1 cells. J. Cell Biol. *193*, 97–108.

Ho Sui, S.J., Fulton, D.L., Arenillas, D.J., Kwon, A.T., and Wasserman, W.W. (2007). oPOSSUM: integrated tools for analysis of regulatory motif over-representation. Nucleic Acids Res. *35* (*Web Server issue, suppl_2*), W245–W252.

Hornsveld, M., Smits, L.M.M., Meerlo, M., van Amersfoort, M., Groot Koerkamp, M.J.A., van Leenen, D., Kloet, D.E.A., Holstege, F.C.P., Derksen, P.W.B., Burgering, B.M.T., and Dansen, T.B. (2018a). FOXO transcription factors both suppress and support breast cancer progression. Cancer Res. *78*, 2356–2369.

Hornsveld, M., Dansen, T.B., Derksen, P.W., and Burgering, B.M.T. (2018b). Re-evaluating the role of FOXOs in cancer. Semin. Cancer Biol. *50*, 90–100.

Hsu, J.Y., Reimann, J.D., Sørensen, C.S., Lukas, J., and Jackson, P.K. (2002). E2F-dependent accumulation of hEmi1 regulates S phase entry by inhibiting APC(Cdh1). Nat. Cell Biol. *4*, 358–366.

Kim, D., Pertea, G., Trapnell, C., Pimentel, H., Kelley, R., and Salzberg, S.L. (2013). TopHat2: accurate alignment of transcriptomes in the presence of insertions, deletions and gene fusions. Genome Biol. *14*, R36.

Kleiblova, P., Shaltiel, I.A., Benada, J., Ševčík, J., Pecháčková, S., Pohlreich, P., Voest, E.E., Dundr, P., Bartek, J., Kleibl, Z., et al. (2013). Gain-of-function

mutations of PPM1D/Wip1 impair the p53-dependent G1 checkpoint. J. Cell Biol. *201*, 511–521.

Koundrioukoff, S., Carignon, S., Técher, H., Letessier, A., Brison, O., and Debatisse, M. (2013). Stepwise activation of the ATR signaling pathway upon increasing replication stress impacts fragile site integrity. PLoS Genet. *9*, e1003643.

Kramer, E.R., Scheuringer, N., Podtelejnikov, A.V., Mann, M., and Peters, J.M. (2000). Mitotic regulation of the APC activator proteins CDC20 and CDH1. Mol. Biol. Cell *11*, 1555–1569.

Krenning, L., Feringa, F.M., Shaltiel, I.A., van den Berg, J., and Medema, R.H. (2014). Transient activation of p53 in G2 phase is sufficient to induce senescence. Mol. Cell *55*, 59–72.

Lee, J., Kim, J.A., Barbier, V., Fotedar, A., and Fotedar, R. (2009). DNA damage triggers p21WAF1-dependent Emil down-regulation that maintains G2 arrest. Mol. Biol. Cell *20*, 1891–1902.

Liu, B., Shats, I., Angus, S.P., Gatza, M.L., and Nevins, J.R. (2013). Interaction of E2F7 transcription factor with E2F1 and C-terminal-binding protein (CtBP) provides a mechanism for E2F7-dependent transcription repression. J. Biol. Chem. *288*, 24581–24589.

Love, M.I., Huber, W., and Anders, S. (2014). Moderated estimation of fold change and dispersion for RNA-seq data with DESeq2. Genome Biol. *15*, 550.

Lukas, C., Savic, V., Bekker-Jensen, S., Doil, C., Neumann, B., Pedersen, R.S., Grøfte, M., Chan, K.L., Hickson, I.D., Bartek, J., and Lukas, J. (2011). 53BP1 nuclear bodies form around DNA lesions generated by mitotic transmission of chromosomes under replication stress. Nat. Cell Biol. *13*, 243–253.

Margottin-Goguet, F., Hsu, J.Y., Loktev, A., Hsieh, H.M., Reimann, J.D., and Jackson, P.K. (2003). Prophase destruction of Emi1 by the SCF(betaTrCP/Slimb) ubiquitin ligase activates the anaphase promoting complex to allow progression beyond prometaphase. Dev. Cell *4*, 813–826.

Medema, R.H., Kops, G.J., Bos, J.L., and Burgering, B.M. (2000). AFX-like Forkhead transcription factors mediate cell-cycle regulation by Ras and PKB through p27kip1. Nature *404*, 782–787.

Meerbrey, K.L., Hu, G., Kessler, J.D., Roarty, K., Li, M.Z., Fang, J.E., Herschkowitz, J.I., Burrows, A.E., Ciccia, A., Sun, T., et al. (2011). The pINDUCER lentiviral toolkit for inducible RNA interference in vitro and in vivo. Proc. Natl. Acad. Sci. USA *108*, 3665–3670.

Miller, J.J., Summers, M.K., Hansen, D.V., Nachury, M.V., Lehman, N.L., Loktev, A., and Jackson, P.K. (2006). Emi1 stably binds and inhibits the anaphase-promoting complex/cyclosome as a pseudosubstrate inhibitor. Genes Dev. *20*, 2410–2420.

Minocherhomji, S., Ying, S., Bjerregaard, V.A., Bursomanno, S., Aleliunaite, A., Wu, W., Mankouri, H.W., Shen, H., Liu, Y., and Hickson, I.D. (2015). Replication stress activates DNA repair synthesis in mitosis. Nature *528*, 286–290.

Mishmar, D., Rahat, A., Scherer, S.W., Nyakatura, G., Hinzmann, B., Kohwi, Y., Mandel-Gutfroind, Y., Lee, J.R., Drescher, B., Sas, D.E., et al. (1998). Molecular characterization of a common fragile site (*FRA7H*) on human chromosome 7 by the cloning of a simian virus 40 integration site. Proc. Natl. Acad. Sci. USA *95*, 8141–8146.

Müllers, E., Cascales, H.S., Jaiswal, H., Saurin, A.T., and Lindqvist, A. (2014). Nuclear translocation of cyclin B1 marks the restriction point for terminal cell cycle exit in G2 phase. Cell Cycle *13*, 2733–2743.

Nakayama, K., Nagahama, H., Minamishima, Y.A., Matsumoto, M., Nakamichi, I., Kitagawa, K., Shirane, M., Tsunematsu, R., Tsukiyama, T., Ishida, N., et al. (2000). Targeted disruption of Skp2 results in accumulation of cyclin E and p27(Kip1), polyploidy and centrosome overduplication. EMBO J. *19*, 2069–2081.

Nakayama, K., Nagahama, H., Minamishima, Y.A., Miyake, S., Ishida, N., Hatakeyama, S., Kitagawa, M., Iemura, S., Natsume, T., and Nakayama, K.I. (2004). Skp2-mediated degradation of p27 regulates progression into mitosis. Dev. Cell *6*, 661–672.

Putker, M., Vos, H.R., van Dorenmalen, K., de Ruiter, H., Duran, A.G., Snel, B., Burgering, B.M., Vermeulen, M., and Dansen, T.B. (2015). Evolutionary acquisition of cysteines determines FOXO paralog-specific redox signaling. Antioxid. Redox Signal. *22*, 15–28.

Rashi-Elkeles, S., Warnatz, H.J., Elkon, R., Kupershtein, A., Chobod, Y., Paz, A., Amstislavskiy, V., Sultan, M., Safer, H., Nietfeld, W., et al. (2014). Parallel profiling of the transcriptome, cistrome, and epigenome in the cellular response to ionizing radiation. Sci. Signal. *7*, rs3.

Reimann, J.D.R., Freed, E., Hsu, J.Y., Kramer, E.R., Peters, J.M., and Jackson, P.K. (2001). Emi1 is a mitotic regulator that interacts with Cdc20 and inhibits the anaphase promoting complex. Cell *105*, 645–655.

Sakaue-Sawano, A., Kurokawa, H., Morimura, T., Hanyu, A., Hama, H., Osawa, H., Kashiwagi, S., Fukami, K., Miyata, T., Miyoshi, H., et al. (2008). Visualizing spatiotemporal dynamics of multicellular cell-cycle progression. Cell *132*, 487–498.

Saldivar, J.C., Cortez, D., and Cimprich, K.A. (2017). The essential kinase ATR: ensuring faithful duplication of a challenging genome. Nat. Rev. Mol. Cell Biol. *18*, 622–636.

Saldivar, J.C., Hamperl, S., Bocek, M.J., Chung, M., Bass, T.E., Cisneros-Soberanis, F., Samejima, K., Xie, L., Paulson, J.R., Earnshaw, W.C., et al. (2018). An intrinsic S/G_2 checkpoint enforced by ATR. Science *361*, 806–810.

Schindelin, J., Arganda-Carreras, I., Frise, E., Kaynig, V., Longair, M., Pietzsch, T., Preibisch, S., Rueden, C., Saalfeld, S., Schmid, B., et al. (2012). Fiji: an open-source platform for biological-image analysis. Nat. Methods *9*, 676–682.

Schmidt, M., Fernandez de Mattos, S., van der Horst, A., Klompmaker, R., Kops, G.J., Lam, E.W., Burgering, B.M., and Medema, R.H. (2002). Cell cycle inhibition by FoxO forkhead transcription factors involves downregulation of cyclin D. Mol. Cell. Biol. *22*, 7842–7852.

Shaltiel, I.A., Krenning, L., Bruinsma, W., and Medema, R.H. (2015). The same, only different - DNA damage checkpoints and their reversal throughout the cell cycle. J. Cell Sci. *128*, 607–620.

Shats, I., Gatza, M.L., Liu, B., Angus, S.P., You, L., and Nevins, J.R. (2013). FOXO transcription factors control E2F1 transcriptional specificity and apoptotic function. Cancer Res. *73*, 6056–6067.

Spencer, S.L., Cappell, S.D., Tsai, F.C., Overton, K.W., Wang, C.L., and Meyer, T. (2013). The proliferation-quiescence decision is controlled by a bifurcation in CDK2 activity at mitotic exit. Cell *155*, 369–383.

Sudo, T., Ota, Y., Kotani, S., Nakao, M., Takami, Y., Takeda, S., and Saya, H. (2001). Activation of Cdh1-dependent APC is required for G1 cell cycle arrest and DNA damage-induced G2 checkpoint in vertebrate cells. EMBO J. *20*, 6499–6508.

Tran, H., Brunet, A., Grenier, J.M., Datta, S.R., Fornace, A.J., Jr., DiStefano, P.S., Chiang, L.W., and Greenberg, M.E. (2002). DNA repair pathway stimulated by the forkhead transcription factor FOXO3a through the Gadd45 protein. Science *296*, 530–534.

Tsai, W.-B., Chung, Y.M., Takahashi, Y., Xu, Z., and Hu, M.C. (2008). Functional interaction between FOXO3a and ATM regulates DNA damage response. Nat. Cell Biol. *10*, 460–467.

Webb, A.E., Pollina, E.A., Vierbuchen, T., Urbán, N., Ucar, D., Leeman, D.S., Martynoga, B., Sewak, M., Rando, T.A., Guillemot, F., et al. (2013). FOXO3 shares common targets with ASCL1 genome-wide and inhibits ASCL1-dependent neurogenesis. Cell Rep. *4*, 477–491.

Wiebusch, L., and Hagemeier, C. (2010). p53- and p21-dependent premature APC/C-Cdh1 activation in G2 is part of the long-term response to genotoxic stress. Oncogene *29*, 3477–3489.

Zachariae, W., Schwab, M., Nasmyth, K., and Seufert, W. (1998). Control of cyclin ubiquitination by CDK-regulated binding of Hct1 to the anaphase promoting complex. Science *282*, 1721–1724.

Zeman, M.K., and Cimprich, K.A. (2014). Causes and consequences of replication stress. Nat. Cell Biol. *16*, 2–9.

CellPress
OPEN ACCESS

STAR★METHODS

KEY RESOURCES TABLE

REAGENT or RESOURCE	SOURCE	IDENTIFIER
Antibodies		
FOXO1	Cell Signaling Technology	CS-2880; RRID: AB_2106495
FOXO3	Novus Biologicals	NB100614; RRID: AB_10001315
P27	BD Biosciences	BD-610241; RRID: AB_397636
P21	BD Biosciences	BD-556430; RRID: AB_396414
P53	Santa Cruz	SC-126; RRID: AB_628082
EMI1	ThermoFisher	3D2D6; RRID: AB_2533333
E2F1	Cell Signaling Technology	CS-3742; RRID: AB_2096936
pRB-S807/811	Cell Signaling Technology	CS-9308; RRID: AB_331472
Cyclin A	Abcam	AB-16726; RRID: AB_302478
Cyclin E	Santa Cruz	SC-198; RRID: AB_631346
Cyclin D	Abcam	AB-134175; RRID: AB_2750906
Cyclin B	Santa Cruz	SC-752; RRID: AB_2072134
CDH1/FZR1	ThermoFisher	MS-1116-P1; RRID: AB_64167
SKP2	Cell Signaling Technology	CS-2652S; RRID: AB_11178941
CHK1	Santa Cruz	SC-8408; RRID: AB_627257
pCHK1-S345	Cell Signaling Technology	CS-2348; RRID: AB_331212
CHK2	Santa Cruz	SC-9064; RRID: AB_2080787
pCHK2-T68	Cell Signaling Technology	CS-2661; RRID: AB_331479
ATM	Abcam	AB-78; RRID: AB_306089
pATM-S1981	Abcam	AB-81292; RRID: AB_1640207
FANCD2	Abcam	AB-108928; RRID: AB_10862535
53BP1	Novus Biologicals	NB-100-304; RRID: AB_10003037
γH2AX	Millipore	MP-05-636; RRID: AB_309864
Anti-HA	Home made	N/A
Anti-GFP	Home made	N/A
Chemicals, peptides, and recombinant proteins		
Aphidicolin	Sigma	A0781
Hydroxyurea	Sigma	H8627
Neocarcinostatin	Sigma	N9162
PKB inhibitor VIII	Chemcruz	SC-202048A
ATR inhibitor VE-821	SelleckChem	S8007
Deposited data		
Raw and analyzed RNA sequencing data	This paper	GEO: GSE159826
Experimental models: cell lines		
hTERT RPE-1	ATCC	CRL-4000; RRID: CVCL_4388
MCF7	ATCC	HTB-22; RRID: CVCL_0031
SKBR3	ATCC	HTB-30; RRID: CVCL_0033
HEK293T	ATCC	CRL-11268; RRID: CVCL_1926
Oligonucleotides		
ON-TARGET siEMI1/FBXO5 SMARTpool	Dharmacon	L-012434
ON-TARGET siCDH1/FZR1 SMARTpool	Dharmacon	L-015377
ON-TARGET siE2F1 SMARTpool	Dharmacon	L-003259
shFOXOs	Broad Institute	TRCN0000020707

(*Continued on next page*)

Continued

REAGENT or RESOURCE	SOURCE	IDENTIFIER
RT-PCR primers	IDT	Table S1
Recombinant DNA		
pINDUCER20	(Meerbrey et al., 2011)	Plasmid #44012; RRID: Addgene_44012
pCW-mTurqouise-EMI1	(Feringa et al., 2016)	N/A
CCNB-YFP	(Krenning et al., 2014)	N/A
53BP1-RFP	(Krenning et al., 2014)	N/A
CSII-EF-mKO2-hCdt1(30/120)	(Sakaue-Sawano et al., 2008)	N/A
CSII-EF-mAG-hGem(1/110)	(Sakaue-Sawano et al., 2008)	N/A
pTON-Flag-eGFP-FOXO1 & FOXO3	(Putker et al., 2015)	N/A
pCDNA3.1-HA-E2F1	(Liu et al., 2013)	N/A
pX330-U6-Chimeric_BB-CBh-hSpCas9	(Cong et al., 2013)	Plasmid #42230; RRID: Addgene_42230
Software and algorithms		
TopHat 2.1.1	(Kim et al., 2013)	https://ccb.jhu.edu/software/tophat/index.shtml
GraphPad	GraphPad	https://www.graphpad.com
ImageJ	(Schindelin et al., 2012)	https://imagej.net/Fiji/
oPOSSUM 3.0	(Ho Sui et al., 2007)	http://opossum.cisreg.ca/oPOSSUM3/
DESeq2	(Love et al., 2014)	http://www.bioconductor.org/packages/release/bioc/html/DESeq2

RESOURCE AVAILABILITY

Lead contact

Further information and requests for resources and reagents should be directed to and will be fulfilled by the Lead Contact, Marten Hornsveld (m.hornsveld@lumc.nl).

Materials availability

All materials and construct used in this study are available upon request. Transfer may require completion of material transfer agreement.

Data and code availability

The mRNA sequencing data generated in this study is available at the NCBI GEO database under GSE159826 (https://www.ncbi.nlm.nih.gov/geo/query/acc.cgi?acc=GSE159826).

This study did not generate new codes.

EXPERIMENTAL MODEL AND SUBJECT DETAILS

Cell lines and generation of cell lines

hTERT-immortalized Retinal Pigment Epithelial cells (RPE-1, female origin), MCF7 breast adenocarcinoma (female origin), SKBR3 breast adenocarcinoma (female origin), 293T Human Embrionic Kidney cells (HEK293T, fetal origin) were obtained from the ATCC and cultured at 37°C and 5% CO_2 in DMEM-F12 (Lonza) containing 10% FBS (Bodinco), 100U/ml penicillin and 100mg/ml streptomycin (Lonza). For doxycycline treatment 200 ng/ml Doxycycline (Sigma) was used for the duration of indicated times. RPE-1 cells in which a fluorescent tag was introduced in one allele of Cyclin B1 (RPE CCNB1^{YFP}) have been described before (Krenning et al., 2014). RPE-CCNB1^{YFP}-53BP1^{mCherry}, RPE CCNB1^{YFP}-EMI1^{mTurq2}-53BP1^{mCherry} cells and RPE-CCNB1^{YFP}-DHB^{mCherry} cells were described before (Feringa et al., 2016). Generation of RPE-FUCCI cells was previously described (Shaltiel et al., 2015). Cells were treated with 0,2 μM, 0,4 μM aphidicolin (Sigma) for the indicated times. 0,2 μM is used to induce replication stress from which cells can recover. 0,4 μM induces a S/G2 arrest and was used to study APC^{CDH1} activation and replication stress checkpoint establishment.

Constructs, lentiviral transduction and transfections

Lentiviral cDNA expression vectors expressing FOXO3.A3 were generated using Gateway cloning in the pINDUCER20 (Meerbrey et al., 2011)(Addgene #44012) doxycycline inducible expression system (Hornsveld et al., 2018a). The lentiviral construct pCW-mTurqouise-EMI1 was generated as previously described(Feringa et al., 2016). Previously generated and characterized

lentiviral doxycycline-inducible pH1tet-flex/FH1tUTG containing shFOXO1/3 (TRCN0000020707) or firefly Luciferase were used for knockdown experiments (de Keizer et al., 2010) (Charitou et al., 2015) (Hornsveld et al., 2018a). Transfection of third generation packaging vectors using Poly-ethylenimine into HEK293T cells generated lentiviral particles. Transfection of pTON-EGFP-FOXO1/FOXO3 (Putker et al., 2015)and pCDNA-HA-E2F1 (Liu et al., 2013) was performed using ExtremeGene 9 (Roche). Transfection of siRNA smartpools targeting *EMI1*, *FZR1*/*CDH1* and *E2F1* was performed using lipofectamine (Life Technologies).

CRISPR/Cas9 mediated knockouts we generated as previously described in (Cong et al., 2013; Blomen et al., 2015). Briefly, pX330 was transfected in for both TP53 and CDKN1A knockout generation. Subsequently, cells were treated with 5 μM Nutlin-3a for 7 days to select out TP53 and CDKN1A deficient cells.

METHOD DETAILS

Immunoblotting and antibodies

For western blot cells are lysed, protein concentration is measured (Bradford, BioRad) and finally dissolved in sample buffer containing 0.2%SDS, 10% glycerol, 0.2% β-mercapto-ethanol, 60mM Tris pH6.8. Equal protein concentrations were loaded and proteins were detected using 6%–15% SDS-PAGE gels and subsequent western-blot analysis with primary antibodies recognizing used 1:2000. Primary antibodies were detected by secondary HRP conjugated antibodies targeting mouse, rabbit, and rat IgG and visualized using chemiluminescence (Biorad) and an ImageQuant LAS 4000 scanner (GE Healthcare). For immunoprecipitation cells transfected with HA-E2F1, GFP-FOXO1, GFP-FOXO3 were lysed in 50mM Tris pH7.4, 150mM NaCl, 1% Triton X-100. For immunoprecipitation Chromotec GFP beads were incubated with cell lysate for 2 h at 4°C, subsequently washed with lysis buffer and boiled in sample buffer. Chromatin-IP was performed as previously described using rabbit anti E2F1 (C-20, SC193) and Rabbit IgG (SC2027) (Eijkelenboom et al., 2013b)

Immunofluorescence

Cells were grown on glass coverslips, fixed using 4% paraformaldehyde and blocked with PBS containing 2% bovine serum albumin (BSA) (Invitrogen) and 0.1% normal goat serum (Invitrogen). Cells were incubated with indicated antibodies (1:500), secondary Alexa488/561 conjugated antibodies and Hoechst (Sigma). Slides were imaged on a Zeiss LSM710 confocal microscope. Quantification of FOXO localization and 53BP1, FANCD2 and γH2AX foci was performed with a custom written ImageJ script that was described previously(Feringa et al., 2016),

RT-qPCR

mRNA was isolated from live cells using the QIAGEN RNeasy kit (QIAGEN) and cDNA synthesis was performed using the iScript cDNA synthesis kit (BioRad). Real-time PCR was performed using Fast Start Universal SYBR Green Master (ROX) mix (Roche) in the CFX Connect Real-time PCR detection system (BioRad). Target genes were amplified using specific primer pairs (Table S1) and specificity was confirmed by analysis of the melting curves. Target gene expression levels were normalized to *GAPDH* and *HNRNPA1* levels.

Flow cytometry

For DNA content profiling and sorting, live cells were incubated with 10 μg/ml Hoechst33342 for 30 min. at 37°C. After incubation cells were trypsinized and transferred to normal culture medium before measuring. mKO-hCDT1, mAG-hGeminin and Hoechst33342 intensity was measured using a BD LSR Fortessa Flow cytometer or BD Aria II FACS (BD bioscience).

Live cell imaging and tracking

20.000 RPE cells were cultured in Lab-Tek II 8-well imaging chambers. Prior to imaging normal culture medium is replaced with Leibovitz medium (Lonza) containing 10% FCS (Lonza),2 mM L-Glutamin, 100U/ml penicillin and 100 μg/ml streptomycin (Lonza). Cells were treated with 0.4 μM aphidicolin and/or doxycycline (Sigma) at indicated time points before imaging. For UV irradiation, medium was aspirated and cells were rinsed with PBS before exposure to global UV irradiation by TUV lamp. After irradiation Leibovitz's L-15 (GIBCO) CO2-independent medium, supplemented with ultra-glutamine, penicillin/streptomycin and 10% fetal calf serum was added to start live-cell imaging as described above. For all experiments where phenotypic outcome was quantified at least 50 cells per condition in each independent biological replicate were scored, $n \geq 50$, unless otherwise stated in figure legends. Imaging was performed on Zeiss Cell observer Real-Time imaging and DeltaVision Elite (applied precision) microscopes for 48 h at 37°C. Cell tracking and quantification was performed using ImageJ (Schindelin et al., 2012). Cells expressing mAG-hGeminin at the moment of doxycycline addition and cell starting to express mAG-hGeminin within 3 h after doxycycline addition were considered S/G2 in the analysis. Relative CDK2 activity and cyclin $B1^{YFP}$ intensity were measured in individual G2 cells that degraded Cyclin B1 after progression through S phase in presence of 0,4μM aphidicolin. Cells were *in silico* alligned at the onset of cyclin B1 degradation and cyclin $B1^{YFP\ value}$s were normalized to the max cyclin B1 level.

mRNA sequencing and Analysis

RPE-1 hTERT cells were synchronized with a double-thymidine block and released in the absence (DMSO) and presence of aphidicolin (DRS) and cultured for 7 h. Subsequently, total RNA from cultured cells was extracted using TRIzol reagent (Invitrogen).

Strand-specific libraries were generated using the TruSeq PolyA Stranded mRNA sample preparation kit (Illumina). In brief, polyadenylated RNA was purified using oligo-dT beads. Following purification, the RNA was fragmented, random-primed and reserve transcribed using SuperScript II Reverse Transcriptase (Invitrogen). The generated cDNA was 3′ end-adenylated and ligated to Illumina Paired-end sequencing adapters and amplified by PCR using HiSeq SR Cluster Kit v4 cBot (Illumina). Libraries were analyzed on a 2100 Bioanalyzer (Agilent) and subsequently sequenced on a HiSeq2000 (Illumina). We performed RNA-seq alignment using TopHat 2.1.1 (Table S2) (Kim et al., 2013). Individual samples were downsampled to 10 million reads, subsequently diferentially expressed genes were indentified by DEseq2 (Love et al., 2014) with an adjusted p value threshold of < 0.005. Transcription factor binding site analysis was performed using oPOSSUM (Ho Sui et al., 2007) (based on JASPAR v7) to determine enrichment for transcription factors by Z-score (effects size) and Fisher exact score (significance) over all human promotors compared to our upregulated genes (Table S2).The following settings were used for the oPOSSUM query; conservation cutoff 0.6, matrix score threshold of 85% and a downstream and upstream region of 10kb around the TSS.

QUANTIFICATION AND STATISTICAL ANALYSIS

All westernblot, RT-PCR, immunofluorescence, live-cell imaging and flow cytometry experiments were performed with technical and biological duplicates or triplicates. Biological replicate sample sizes (n = x) and other experiment-specific details are indicated in the figure legends. Data were plotted and analyzed using GraphPad. Data are represented as the mean of multiple replicates ± SD or SEM. Violin plots include the Median (solid line) and upper and lower quartiles (dashed line). For Figures 1D, 2C, 3D–3F, and S1A statistical significance was determined by Welch's corrected unpaired Student's t test's. Differences between samples were considered significant at $p \geq 0.05$ (*) ($p \geq 0.005$ **, $p \geq 0.0005$ ***, $p \geq 0.00005$ ****). Statistical significance for Figure 3H was determined using Bonferonni Multiple testing corrected ANOVA and significance assumed at $p \geq 0.05$ = (*), ($p \geq 0.005$ = ***, $p \geq 0.0005$ = ****). Detailed description of the statistical analysis of mRNA requencing data in Figures 2 and S2 is provided in the "mRNA sequencing and Analysis" section of the "Method Details."